THE ASTROPHYSICAL JOURNAL, 339:268–278, 1989 April 1

INTERACTING WINDS AND THE SHAPING OF PLANETARY NEBULAE

NOAM SOKER
Department of Astronomy, University of Virginia
AND
MARIO LIVIO
Department of Physics, Technion
Received 1988 May 20; accepted 1988 September 9

ABSTRACT

Using two-dimensional hydrodynamics, we investigate the problem of shaping of planetary nebulae by the interacting winds model. We obtain the shock structure and demonstrate that interacting winds are capable of producing morphologies similar to the ones observed in planetary nebulae, provided that a density contrast exists between the equatorial and polar directions. This confirms recent suggestions by Balick. We discuss mechanisms that can produce the required density contrast and show that binary central stars provide the most natural mechanism, especially via common envelope evolution. It is not yet entirely clear whether stellar rotation is sufficient to generate the required contrast in the case of single central stars. We finally point out that interacting winds may play an important role in SN 1987A.

Subject headings: hydrodynamics — nebulae: planetary — shock waves — stars: winds

I. INTRODUCTION

The interacting winds model (e.g., Weaver *et al.* 1977; Kwok 1982; Kahn 1983) for the shaping of planetary nebulae has had considerable success in explaining various features in the morphology of planetary nebulae (PNs). In this model, the hot central star of the PN emits a (low-density) fast wind at a velocity of the order of 1000 km s^{-1}. This fast wind "catches up" with the slow wind resulting from the ejection of the progenitor red giant's envelope (moving at ~ 10 km s^{-1}) and drives a shock wave into it. This "snow plowing" results in a bright shell and also has various dynamical consequences. Balick (1987) has suggested a morphological classification of PNs, ranging from spherical, through elliptical, to "butterfly." He proposed that the different morphologies that are observed, result from a difference in the "density contrast" in the slow wind between the equatorial and polar directions. According to his suggestion, a relatively moderate contrast produces an elliptical shell, while a strong contrast results in a "butterfly" shape.

Balick, Preston, and Icke (1987) have extended Balick's original idea and suggested that the fast wind can be collimated by the inner shock and that the interacting winds can produce the ansae (knots) observed in some PNs.

On a different front, recent calculations of the common envelope (CE) phase in the evolution of binary systems, have demonstrated that the ejected envelope is concentrated toward the orbital plane (Livio and Soker 1988). This result, obtained in a three-dimensional hydrodynamical calculation, confirms the original prediction of Livio, Salzman, and Shaviv (1979) and Livio (1982) and agrees with the results of two-dimensional hydrodynamical calculations (Bodenheimer and Taam 1984). Furthermore, Livio and Soker (1988) have identified the conditions that can lead to various degrees of density contrast between the equatorial (orbital plane) and polar directions. In general, it was found that if the spiraling-in process occurs inside the envelope of a highly evolved AGB star (very centrally condensed), then a relatively mild contrast ensues. A high contrast results from less evolved (less centrally condensed) AGB stars or from normal giants. Thus, CE evolution is a natural agent, capable of producing the density contrast upon which the interacting winds model can operate, to produce different morphologies (in PNs containing binary nuclei).

Bond and Livio (1988) examined CCD images of all the PNs with binary nuclei and have shown them to be qualitatively consistent with the picture emerging from the combined action of CE evolution and interacting winds shaping. In the present, still preliminary work, we take the interacting winds model a step further and calculate time-dependent flow patterns resulting from interacting winds, using two-dimensional hydrodynamics. With Balick's classification scheme and the results of CE evolution in mind, we calculate the configurations obtained for different density contrasts. The method of calculation and some test runs are described in § II. The results of the numerical calculations are presented in § III and discussed in § IV.

II. METHOD OF CALCULATION AND NUMERICAL TESTS

We used a pseudo-particle description of the hydrodynamics, which is a modified two-dimensional version of the three-dimensional scheme described by Livio *et al.* (1986*b*) and Soker *et al.* (1987). We shall therefore not repeat the technical details here. For the parameter α, which determines the strength of the interparticle interaction, we used $\alpha = 1$ in the primary grid and $\alpha = 0.3$ in the secondary grid (see Livio *et al.* 1986*a* for the two-grid method of intercell interactions). For the distribution of specific internal energy among the particles we used the same value of α as for the interparticle interaction in each grid (see, e.g., Hensler 1982). These values were found to produce the best results in the test runs to be described presently. We did not attempt to solve the radiative transfer problem, in particular the effects of the ionizing radiation from the central star were not treated.

Tests of the numerical scheme related to accretion problems

are described in Livio *et al.* (1986*a*). In order to test the scheme in relation to the interacting-winds problem we performed a few spherically symmetric calculations, which allowed us to compare the results with those obtained from self-similar solutions (Chevalier and Imamura 1983; see also Giuliani 1981; Kwok 1982).

In the first test calculation, we assumed a slow wind characterized by a mass loss rate of $\dot{M}_1 = 10^{-5}\ M_\odot\ \mathrm{yr}^{-1}$ and a velocity of $V_1 = 10\ \mathrm{km\ s}^{-1}$ and a fast wind of $\dot{M}_2 = 10^{-6}\ M_\odot\ \mathrm{yr}^{-1}$ and $V_2 = 1000\ \mathrm{km\ s}^{-1}$. The mass-loss rate in the fast wind is higher than that emanating from the hot central star of PNs, its value for the test run was taken for numerical convenience only. The transition time between the end of the slow wind and the beginning of the fast wind was taken as 1000 yr. A Mach number of 4 was assumed for both winds. We used a grid of 192 × 192 cells, calculating only $\frac{1}{4}$ of the symmetry plane. The calculation used 205,800 particles in the slow wind and 150 particles were injected every time step (corresponding to 1.5×10^7 s) in the fast wind. The flow configuration is characterized by an inner shock, an outer shock and a contact discontinuity (see, e.g., Chevalier and Imamura 1983). In the run, we found that some numerical problems developed at the inner shock. Due to the fact that the pressure gradient in that region is very large, while the density is quite low (of the order of 10^{-3} of that in the slow wind), some particles developed negative velocities (toward the hot star). Consequently, a region of low Mach number developed, which the scheme could not handle (e.g., Harlow 1964). Since the total mass involved in this motion constituted no more than a few percent of the mass flowing into the outer shock, we removed it from the calculation. This acts effectively as very efficient cooling of the fast wind at the inner shock, or as leakage of hot gas from the inner hot bubble. Such a leakage may have actually been observed in the case of the ring nebula NGC 6888 (Raymond 1988; Bochkarev 1988). The main effect of this numerical procedure has been to bring the inner shock closer to the contact discontinuity than in the self-similar solutions. Nevertheless, as we shall soon see, most of the results are not significantly affected and our overall energy nonconservation does not exceed a few percent.

For the purpose of comparison of our results with the self-similar solutions, we denote by S_1 the velocity of the outer shock, by R_1 the radius of that shock and by R_c the radius of the contact discontinuity (location of maximal density) between the outer and inner shocks (R_2 is the inner shock radius). The maximum gas velocity after the outer shock is denoted by V_{max}. Table 1 compares our numerical results with those obtained in the self-similar solutions of Chevalier and Imamura (1983) and for S_1 also with Kwok (1982). As can be seen from Table 1, the numerical results agree with the self-similar ones to within a few percent for most quantities. The relatively larger discrepancy in the pressure is caused by the removal of mass (and energy) as described above. As already noted, this effective "cooling" brings the inner shock closer to the contact discontinuity. Similar results were obtained in a second test run in which we took $\dot{M}_1 = 10^{-5}\ M_\odot\ \mathrm{yr}^{-1}$ and $\dot{M}_2 = 2 \times 10^{-7}\ M_\odot\ \mathrm{yr}^{-1}$. Consequently, we believe that the adopted numerical scheme is quite adequate for the determination of the morphology arising from the interacting winds model. Numerical values, however, should be treated with caution.

All the calculations were performed on the CRAY X-MP/48 supercomputer at the Pittsburgh Supercomputing Center.

TABLE 1

COMPARISON WITH SELF-SIMILAR SOLUTIONS

Physical Quantity	Self-Similar Value	Numerical Value	Reference
S_1[a]	90 km s^{-1} 75.4 km s^{-1}	77 km s^{-1}	1, 2
R_c/R_1[b]	0.86	0.9	1
V_{max}/S_1[c]	0.86	0.83	1
$P_{\mathrm{max}}/\rho_1 V_1^2$[d]	52	46	1
R_c/R_2[e]	2.8	1.6	1

[a] S_1 velocity of outer shock.
[b] R_c: radius of contact discontinuity, R_1: radius of outer shock.
[c] V_{max}: maximum velocity in the shell.
[d] P_{max}: maximum pressure in the shell; ρ_1, V_1: density and velocity of the slow wind.
[e] R_2: radius of inner shock.
REFERENCES.—(1) Chevalier and Imamura 1983, (2) Kwok 1982.

III. NUMERICAL RESULTS

We assumed the following parameters in the calculation: $\dot{M}_{\mathrm{slow}} = 10^{-5}\ M_\odot\ \mathrm{yr}^{-1}$, a velocity of $V_{\mathrm{slow}} = 10\ \mathrm{km\ s}^{-1}$ and a Mach number $M_{\mathrm{slow}} = 5$. For the fast wind we took $\dot{M}_{\mathrm{fast}} = 2 \times 10^{-7}\ M_\odot\ \mathrm{yr}^{-1}$, $V_{\mathrm{fast}} = 1000\ \mathrm{km\ s}^{-1}$, and $M_{\mathrm{fast}} = 40$. These values are in the range expected for PN formation (e.g., Volk and Kwok 1985; Iben 1984; Perinotto 1983). The fast wind was started 2300 yr after the end of the slow wind (Schonberner 1983; Volk and Kwok 1985). For the specific heats ratio we used $\gamma = 5/3$ and $\gamma = 1.1$ (the latter value in order to simulate a situation in which more significant cooling has taken place). We performed two runs with a density contrast. For the density profile we have assumed the functional form (e.g., Kahn and West 1985)

$$\rho = \rho_0(1 + a\cos^n\theta)\,, \quad \begin{array}{l} a = 15\ n = 4\,, \\ \quad \text{high-density contrast} \\ a = 5\ n = 4\,, \\ \quad \text{low-density contrast} \end{array} \tag{1}$$

where θ is the angle to the x-axis, which is taken to be in the equatorial plane. The y-axis is taken to be along the polar direction, which is the symmetry axis. In Figures 1*a*–1*c* we show the time development of the density contours for the high-density contrast and $\gamma = 5/3$. The velocity field is presented in Figures 2*a*–2*d*. We can see that at $t = 950$ yr ($t = 0$ denotes the start of the fast wind) the fast wind generates a compression and a large density gradient in the equatorial direction, while it plunges into the (relatively dilate) slow wind in the polar direction (Figs. 1*a*, 2*a*, and 2*b*). Some higher density knots start forming (by compression of relatively cool material) in the polar direction. Consequently, we observe the appearance of a bow shock, formed by the motion of these knots (e.g., Fig. 2*a*). The inner shock is also clearly seen in Figure 2*a*. The outer shock at $t = 950$ yr (close to the outer edge in the polar direction) is best seen in Figure 2*b* (which describes the velocity field at the same time, but on a different scale). At a somewhat later time ($t \simeq 1400$ yr) the material that has been accelerated by the fast wind, starts penetrating the spherical shell formed by the slow wind (e.g., Figs. 1*b* and 2*c*). At $t = 1900$ yr the fast material has penetrated the slow wind, and it forms some kind of "bubbles" (or "jets") in the polar direction (Figs. 1*c* and 2*d*). This phase is accompanied by the development of a Rayleigh-Taylor instability (see also Kahn 1983), very similar to the one obtained in the evolution of a

superbubble in the ISM (e.g., MacLow, McCray, and Norman 1988, compare to our Fig. 2*d*). At the same time, a high-density ring, which appears as two arcs when projected, remains in the equatorial direction. In Figure 3 we show the flow structure for the high-density contrast case at $t = 950$ yr. We present the inner shock, the outer shock, the bow shock, and the high-density line, which corresponds to the contact discontinuity in the self-similar solution. The exact position of the bow shock is somewhat uncertain, due to numerical limitations. It is possible that what we observe here is really the formation of a dome-shaped shock, as a result of the operation of a de Laval nozzle. The position of the shock also changes with time. The main difference between the results of the run with $\gamma = 1.1$ and the one with $\gamma = 5/3$, is that the structure evolves faster for $\gamma = 5/3$ (the pressure being higher) but otherwise the configurations obtained are quite similar.

The results for the low-density contrast $\gamma = 5/3$ case, are presented in Figures 4*a*–4*d* and 5*a*–5*c*. Like in the previous run, we have used 160,000 particles in the slow wind, 750 particles were injected every time step in the fast wind, the time step was 3×10^7 s and the cell size 3×10^{15} cm.

We again observe the structure of an inner and outer shock and a bow shock formed by the motion of high-density knots, or a shock formed by a de Laval nozzle, (e.g., Figs. 4*a*, 5*a*, and 5*b*). In this case, the compressed shell is still intact (and elliptical) at $t = 1520$ yr and the "bubbles" in the polar direction form only at $t \approx 2700$ yr (compared to ~ 1400 yr in the case of the higher density contrast). Again, two arcs form (in the projected image) in the equatorial direction. While from the point of view of comparison with CCD photographs (most of which are of evolved PNs), it would have been useful to continue the runs to later times, the memory and time requirements on the computer become prohibitive.

IV. DISCUSSION

A key ingredient for the production of the morphologies obtained in the present work, which agree extremely well with the classification proposed by Balick (1987), is the existence of a density contrast between the equatorial and polar directions. Such a contrast, capable of producing a variety of shock cross sections (Kahn and West 1985) is observed in many PNs (Balick, Preston, and Icke 1987). Another prediction of the interacting winds model, confirmed by our hydrodynamical calculations and by observations, is the production of knots (ansae) near the sharp ends of elliptical nebulae (e.g., Figs 1*a*–1*c*). These knots are produced when higher density regions are formed along the long axis of the ellipse. In turn, these knots cool and recombine more easily.

It is important to note that our calculations treat only the hydrodynamical aspects of the interacting winds model and

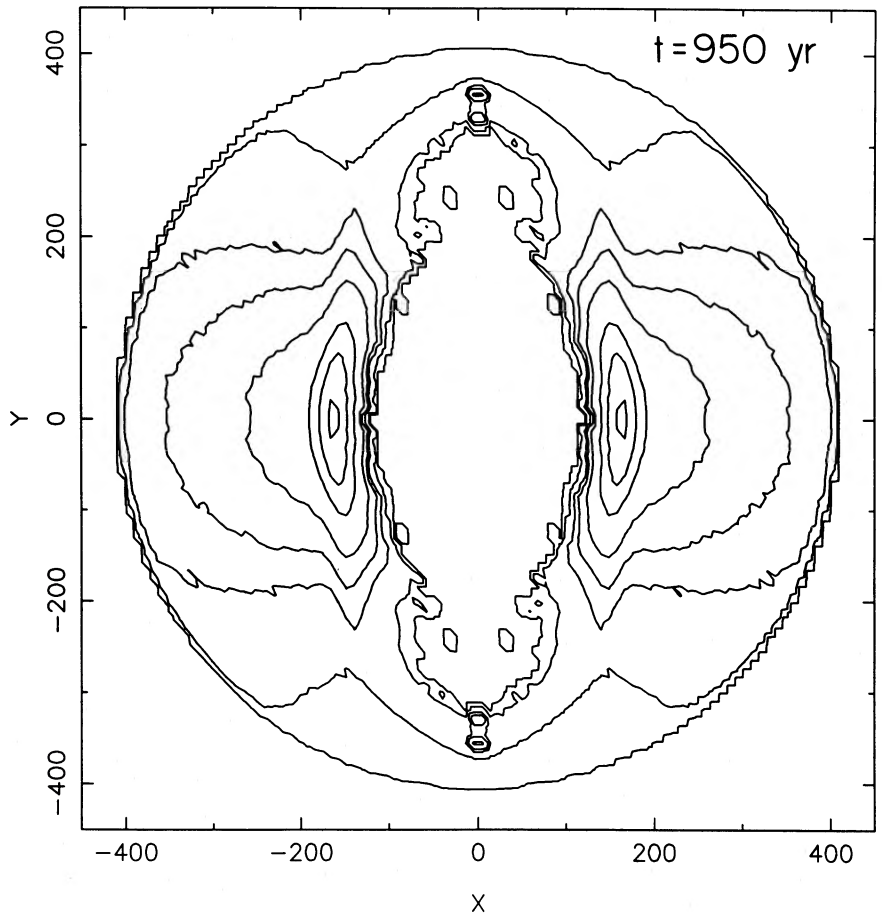

FIG. 1*a*

FIG. 1.—(*a*) Density contours for the high-density contrast case (see eq. [1]) at time $t = 950$ yr from the start of the fast wind (at $r = 60 \times 10^{15}$ cm in our calculations). The units on the axes are 10^{15} cm, and the density levels, in units of 10^{-22} g cm^{-3}, are: 0.1, 1, 4, 7, 13, 29, 45, and 61.

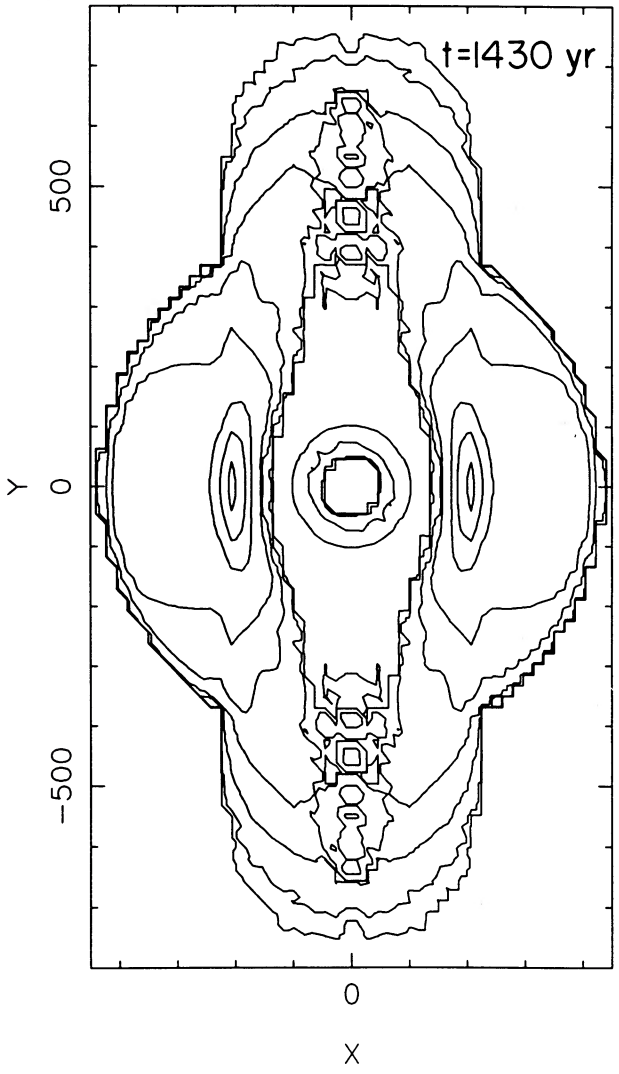

FIG. 1b

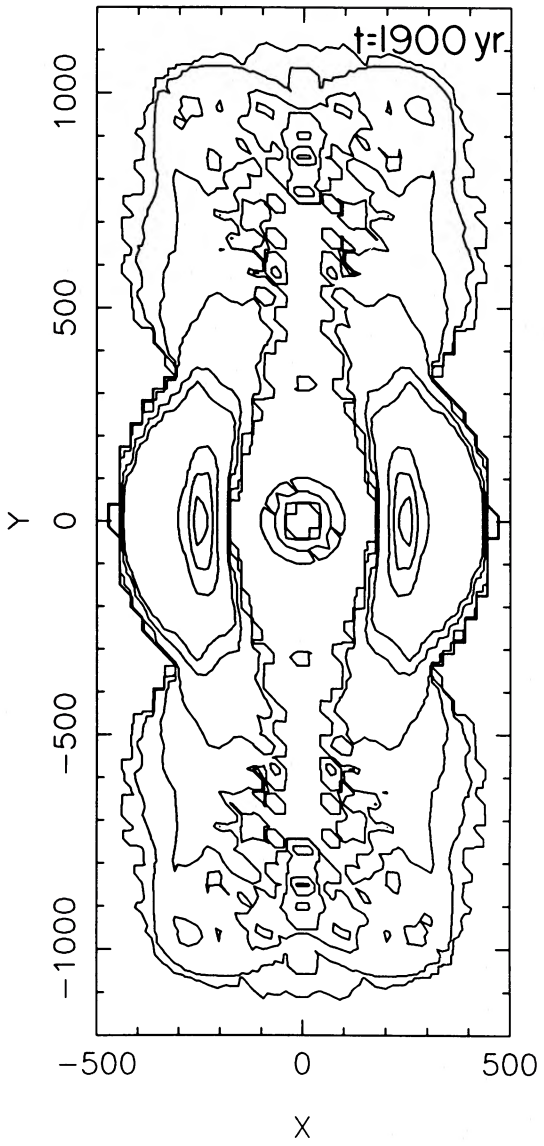

FIG. 1c

FIG. 1.—(*b*) The same as Fig. 1*a*, at $t = 1430$. The innermost contour is where the fast wind starts. The density levels in units of 10^{-22} g cm^{-3} are 0.0001, 0.001, 0.01, 0.1, 1, 3.5, 17, 30, and 43. (*c*) The same as Fig. 1*c* at $t = 1900$ yr. The density levels in units of 10^{-22} g cm^{-3} are 0.0001, 0.001, 0.01, 0.1, 1, 2, 11, 20, and 29.

completely ignore the effects of the ionizing radiation from the central star. Extreme caution should therefore be exercised in attempting to relate the figures obtained in the present work to the images of PNs. We note, however, one difference between the present results and the picture predicted by Balick, Preston, and Icke (1987). The knots form already between the inner and outer shocks, and therefore the bow shock associated with them is located (at least part of the time) between these shocks. In the Balick *et al.* picture, the knots and the bow shock are outside the outer shock.

In spite of this difference and the above caveat concerning the comparison to CCD images of PNs, one cannot avoid noticing the striking similarity between Figures 1*a*–1*c* and 4*a*–4*c* and the CCD images of some PNs (e.g., NGC 6826, NGC 3242, NGC 7009; Balick 1987). This similarity leads us to the speculative suggestion that maybe the sharp edge of the outer halo represents the outer shock after all, with the outer halo itself being shocked slow wind material. This suggestion may be supported by the following observation. If the knots were outside the outer shock (as in the Balick *et al.* picture) then the edge of the outer halo should mark unshocked slow wind material. Since the outer halo is elongated in the polar direction, this seems to require higher velocities (of the slow wind) in the polar direction (unless of course the sharp edge is formed by ionization only). While higher velocities in the polar direction may be expected in the case of rotating stars (e.g., Poe and Friend 1986, but see discussion below), this is *definitely not the case* in the ejection of a CE. Since at least some of the better examples of this morphology (e.g., NGC 6826) may represent PNs with binary central stars, the possibility that the sharp outer edge of the outer halo marks the position of the outer shock should be considered (further support to this possibility can perhaps be found in NGC 7009 where the knots appear outside the outer halo as in, e.g., Figs. 1*b* and 1*c* in our calculation).

Since PN shaping appears to rely so heavily on the presence

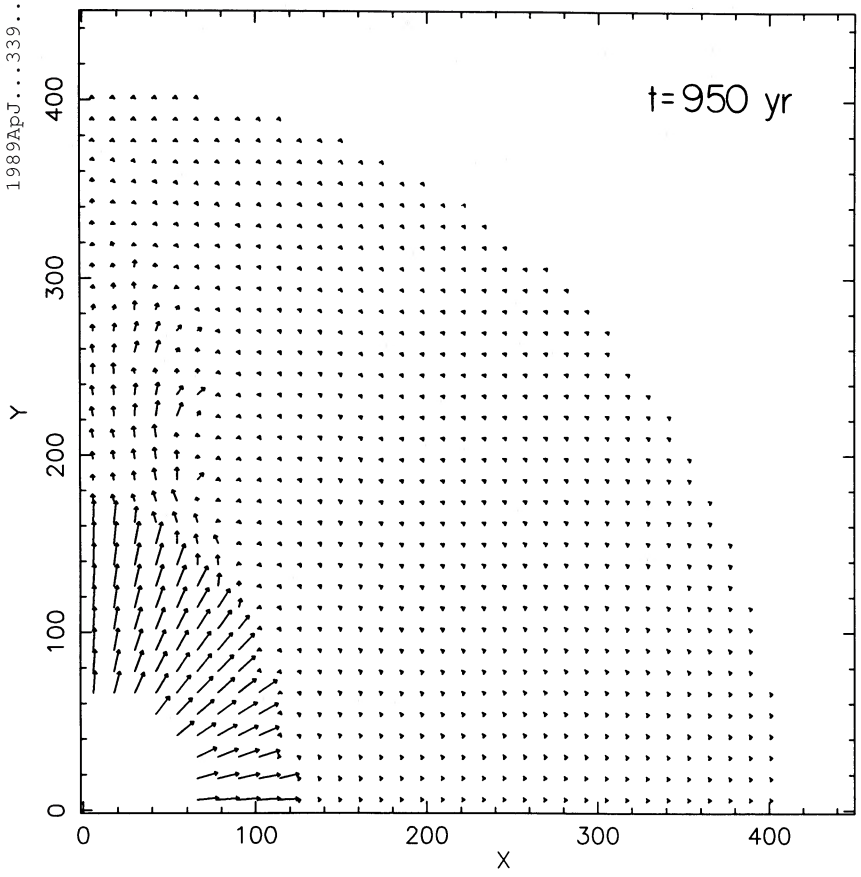

FIG. 2*a*

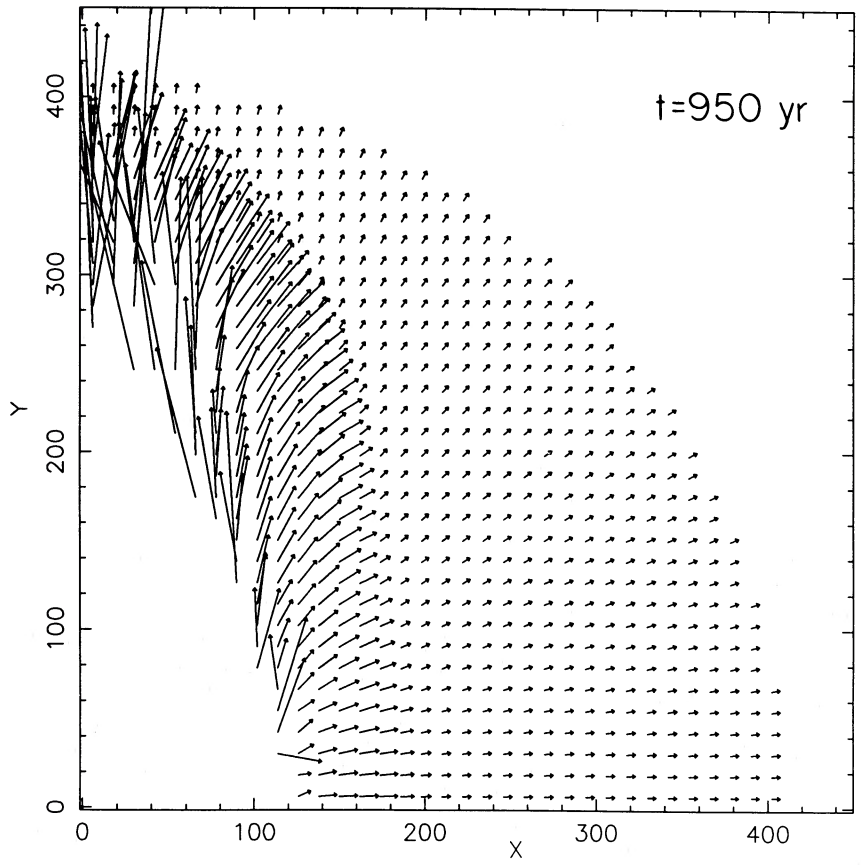

FIG. 2*b*

FIG. 2.—(*a*) The velocity field corresponding to the high-density contrast case (see eq. [1]) at time $t = 950$ yr. Each unit length (as measured on the axes) of the arrows corresponds to a velocity of 80 km s^{-1}. (*b*) The same as (*a*), with each unit length (as measured on the axes) of the arrows corresponding to a velocity of 2 km s^{-1}.

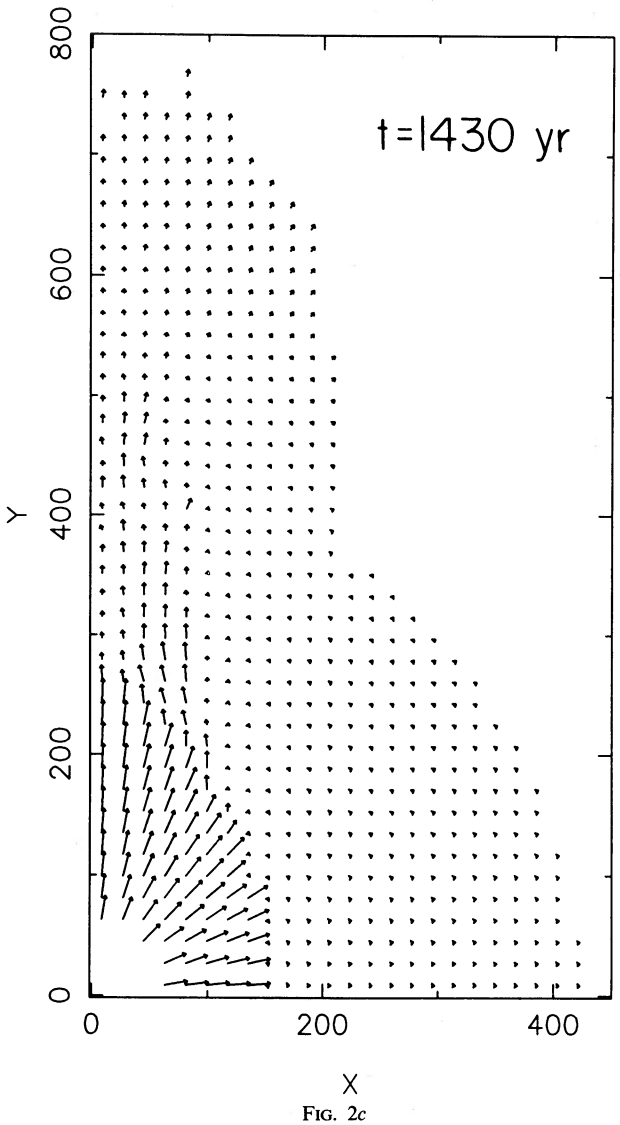

FIG. 2c

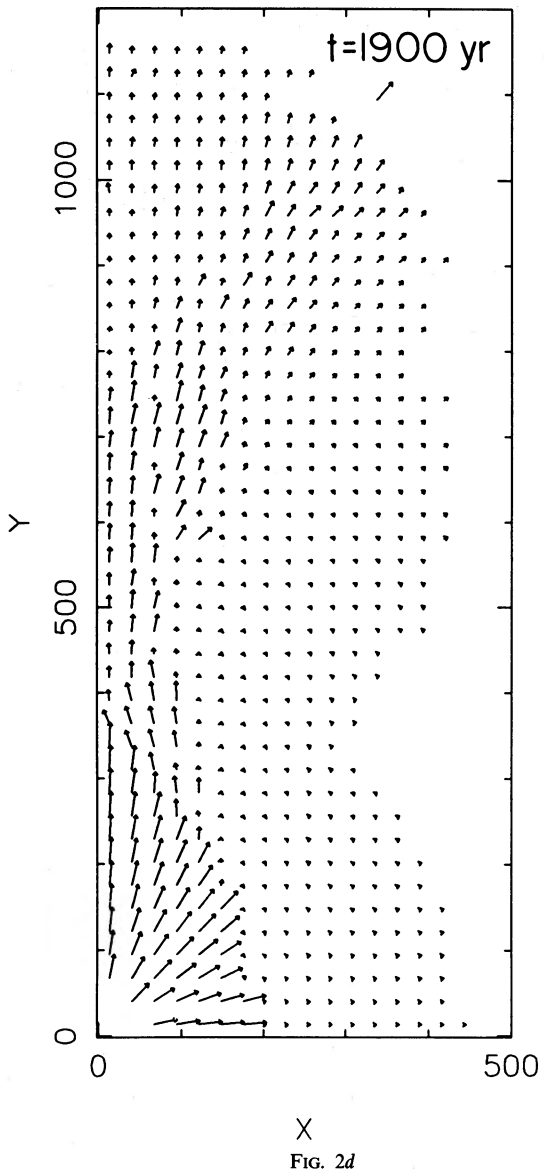

FIG. 2d

FIG. 2.—(*c*) The same as Fig. 2*a* at $t = 1430$ yr. Each unit length of the arrows corresponds to a velocity of 50 km s^{-1}. (*d*) The same as Fig. 2*a*, at $t = 1900$ yr. Each unit length of the arrows corresponds to a velocity of 35 km s^{-1}.

of a density contrast it is important to attempt to establish the physical cause for the generation of such a contrast. In Balick's observations, ~10 PNs (out of 51) were found to possess a butterfly morphology (requiring a high-density contrast), ~20 were found to be elliptical (requiring a somewhat milder contrast) and ~10 were found to be round (no density contrast). It should be noted that in the present calculation, in the high-contrast case, the ratio of the densities in the equatorial and polar directions is 16 (eq. [1]). In the low-contrast case it is 6. If we look at the mass contained in a cone, within 20° of the rotation axis, then for the high-contrast case it is only ~0.1 of that obtained for spherically symmetric ejection (it is ~0.3 for the low-contrast case). Livio and Soker (1988) and Bodenheimer and Taam (1984) have demonstrated how in the case of PNs with binary central stars, the density contrast is generated by the ejection of the CE. Livio and Soker have also identified the configurations from which various degrees of contrast can be obtained. Extreme contrasts result from not very centrally condensed configurations (not very evolved AGB stars or normal giants) and relatively massive secondary stars. Mild contrasts are obtained from very centrally condensed configurations (highly evolved AGB stars). A different scenario for producing contrasts in wide binaries, in which the giant never fills its Roche lobe was suggested by Kolesnik and Pilyugin (1986). The morphology expected for PNs with close binary nuclei is consistent with the observed morphologies (Bond and Livio 1989). The fraction of PNs with close binary nuclei (in which one component fills its Roche lobe after hydrogen or helium is exhausted in its core) has recently been estimated to be of the order of 15%–20% (Iben and Tutukov 1988). If we add to this possible shaping in wide binaries, (in which nevertheless the orbital velocity of the secondary must exceed the nebular expansion velocity), perhaps as many as ~50% of all PNs could experience this type of shaping (all binaries with an

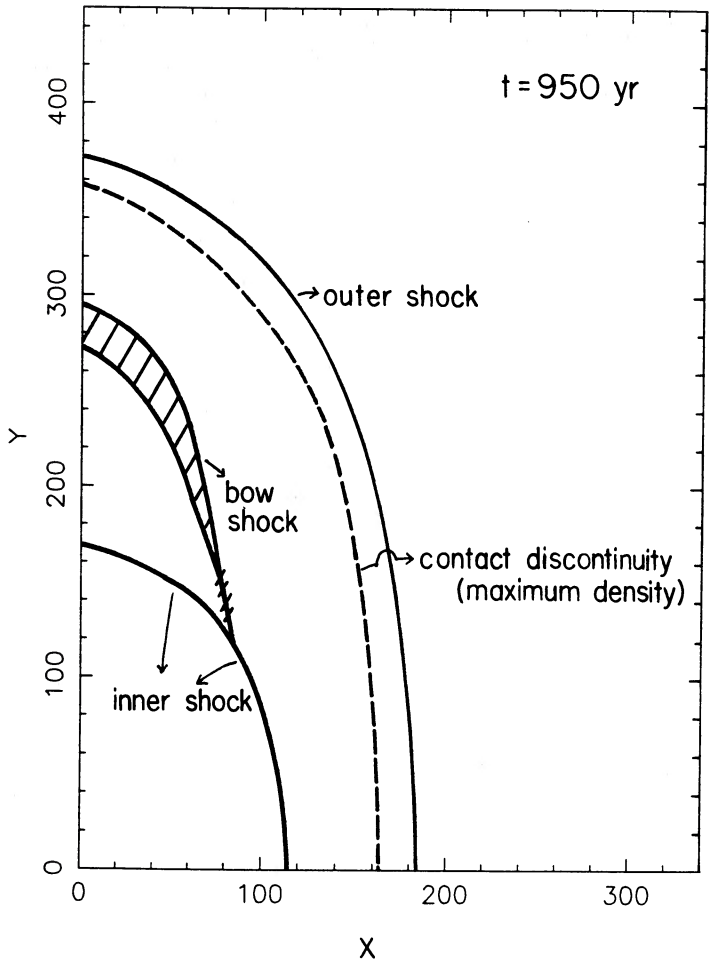

FIG. 3.—The structure of the flow for the case of a high-density contrast, at time $t = 950$ yr. The position of the "bow" shock is uncertain and time dependent. Its dome-shaped part may be formed by the operation of a de Laval nozzle (*see text*).

initial separation $a_0 \lesssim 10{,}000 R_\odot$). Nevertheless, clearly not all PNs possess binary nuclei, and thus other mechanisms must be invoked for producing a density contrast (or for shaping not in the context of the interacting winds model). Another mechanism capable (in principle at least) of generating a density contrast is stellar rotation. Indeed, it has been shown that rotation can produce an equatorial density enhancement of up to a factor of 5 (compared to the polar direction, Poe and Friend 1986). Calvert and Peimbert (1983) have suggested that the "butterfly" morphology is related to rapid rotation. However, as pointed out by Zuckerman and Gatley (1987), by the time the star expands to become an AGB star, its surface velocity is very likely to be a very small fraction of the escape velocity, thus, making a large effect of the rotational velocity on the mass-loss rate implausible. It should also be noted that no evidence was found for a dependence of the mass-loss rate on rotational velocity (Friend and Abbott 1986). On the other hand, *IRAS* observations (Waters 1986) do seem to indicate mass-loss rates around the equator, that are considerably higher than those found from *IUE* observations.

Before concluding we would like to mention (somewhat speculatively) that the results presented in this paper can also have important consequences for SN 1987A, if rapid rotation (or some other mechanism) produced a density contrast in the envelope material lost from the progenitor. A rotation of the progenitor's envelope, can explain the asymmetry in the expanding SN envelope following the explosion (Chevalier and Soker 1989), which is probably responsible for the observed polarization. It should also be noted that rapid rotation has been invoked (Weiss, Hillebrandt, and Truran 1988) as a possible agent for producing (via meridional circulation) the high N/C and N/O ratios detected by *IUE* (Cassatella 1987; Blakes *et al.* 1987). If such a density contrast indeed exists, the supernova ejecta would interact with the envelope matter (lost by the progenitor) much in the same way as described by the results of the present work. Therefore, a similar morphology may be expected for the flow.

To conclude, using two-dimensional hydrodynamics we have demonstrated that the interacting winds model is capable of producing morphologies similar to those observed in PNs, provided that there exists a density contrast in the slow wind, between the equatorial and polar directions. Common envelope evolution produces the necessary density contrast, in the case of PNs with close binary nuceli. Wider binary central stars may also act to ensure the generation of such a contrast, thus accounting together for up to 50% of all PNs. It is not yet entirely clear whether stellar rotation can produce the required equatorial density enhancement.

Interacting winds may play a similar role (to that they play in PNs) in the shaping of the remnant of SN 1987A.

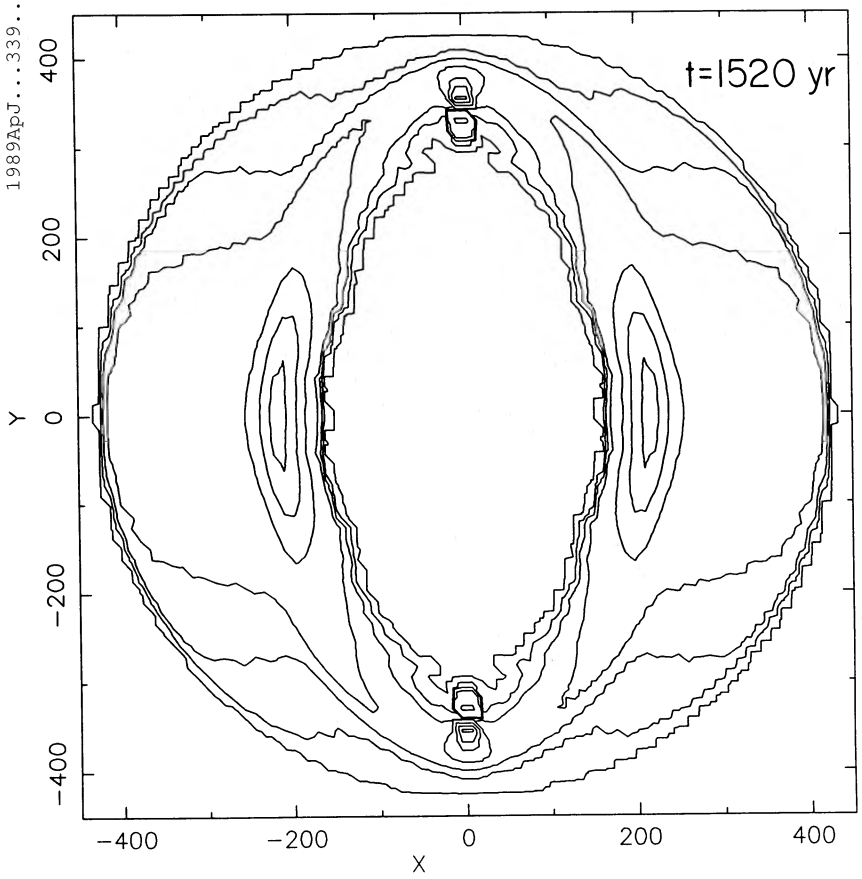

FIG. 4*a*

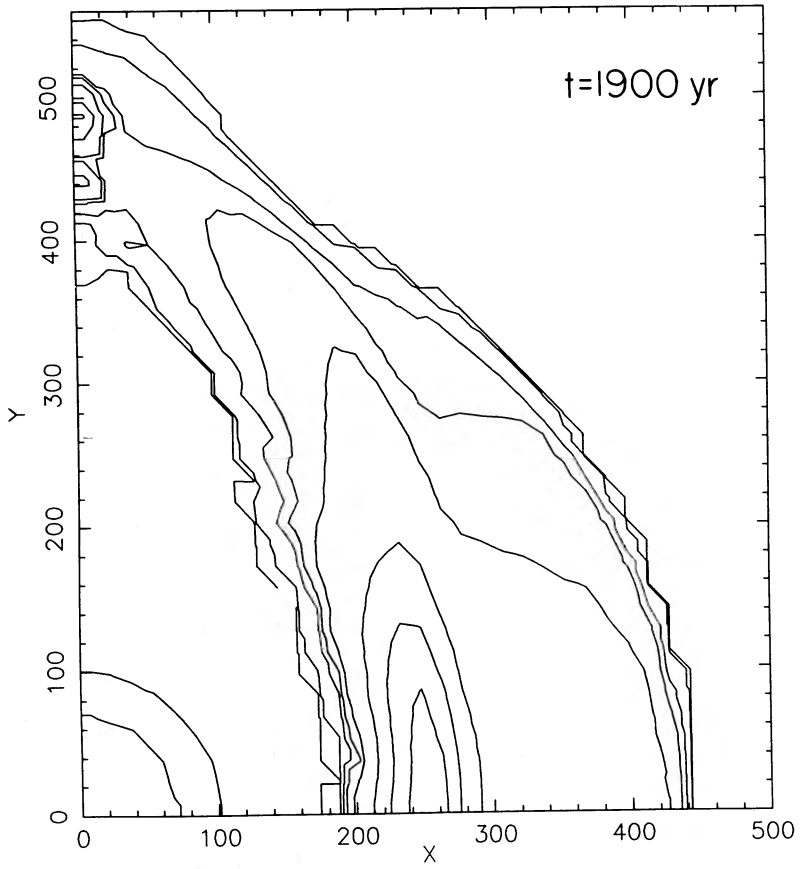

FIG. 4*b*

FIG. 4.—(*a*) Density contours for the low-density contrast case (see eq. [1]) at time $t = 1520$ yr from the start of the fast wind. The units on the axes are 10^{15} cm and the density levels, in units of 10^{-22} g cm^{-3}, are 0.1, 1, 2, 4, 15, 26, and 37. (*b*) The same as (*a*) at $t = 1900$ yr and an expanded scale. The density levels, in units of 10^{-22} g cm^{-3}, are 0.01, 0.1, 1, 2, 4, 12, 20, and 28.

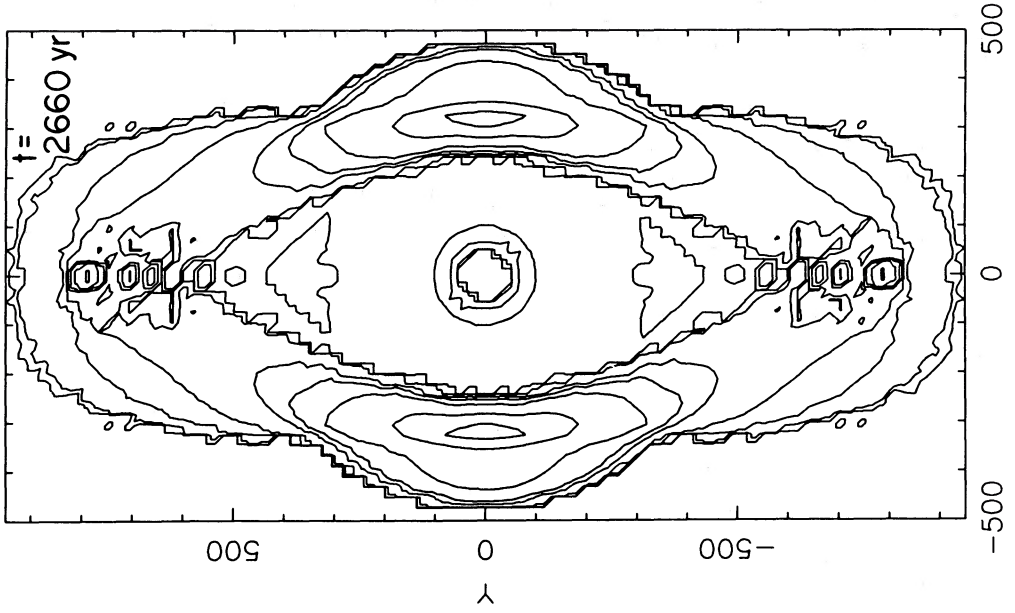

FIG. 4d

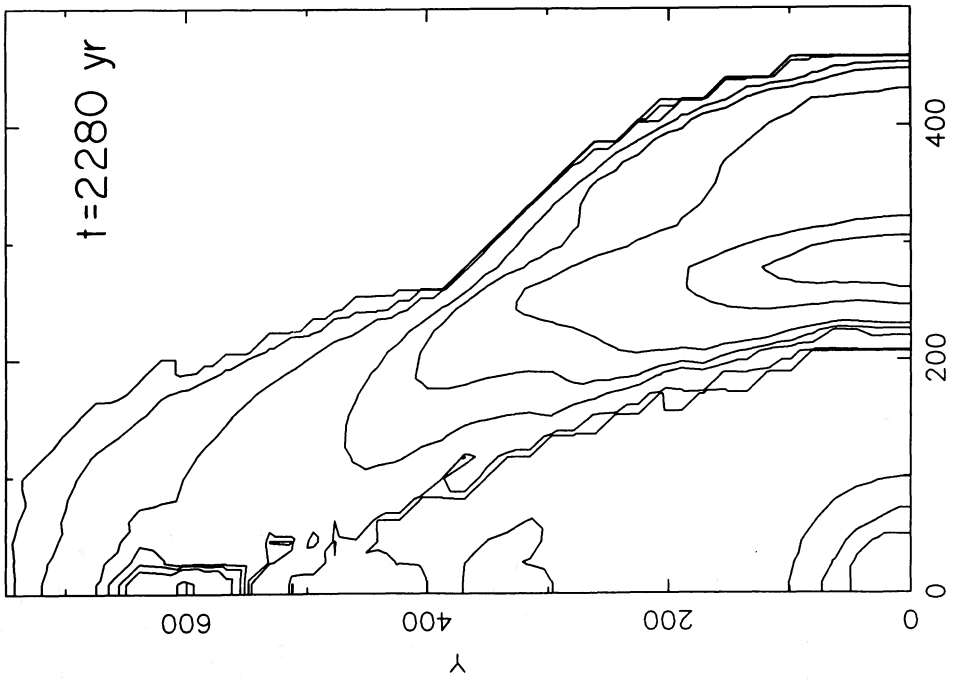

FIG. 4c

FIG. 4.—(c) The same as Fig. 4b at $t = 2280$ yr. The density levels in units of 10^{-22} g cm^{-3} are 0.001, 0.01, 0.1, 1, 2, 4, 12, and 20. (d) The same as Fig. 4a at $t = 2660$ yr. The density levels, in units of 10^{-22} g cm^{-3} are 0.0003, 0.001, 0.01, 0.1, 1, 2, 4, 12, and 20.

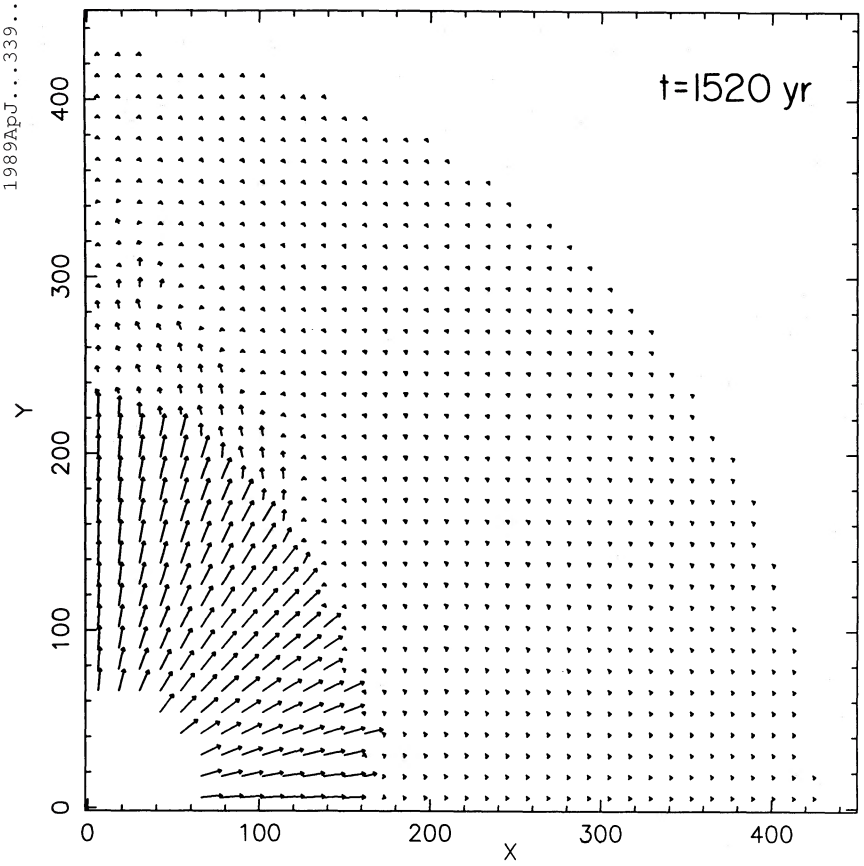

FIG. 5a

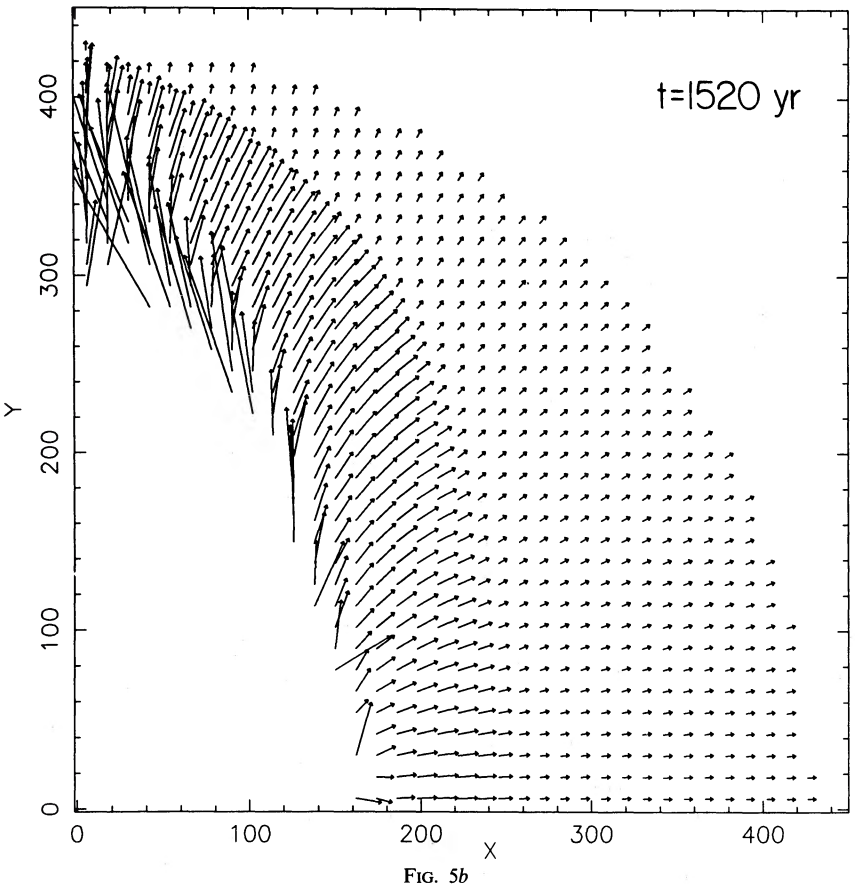

FIG. 5b

FIG. 5.—(*a*) The velocity field corresponding to the low-density contrast case (see eq. [1]) at time $t = 1520$ yr. Each unit length (as measured on the axes) of the arrows corresponds to a velocity of 80 km s^{-1}. (*b*) The same as Fig. 5*a*, with each unit length (as measured on the axes) of

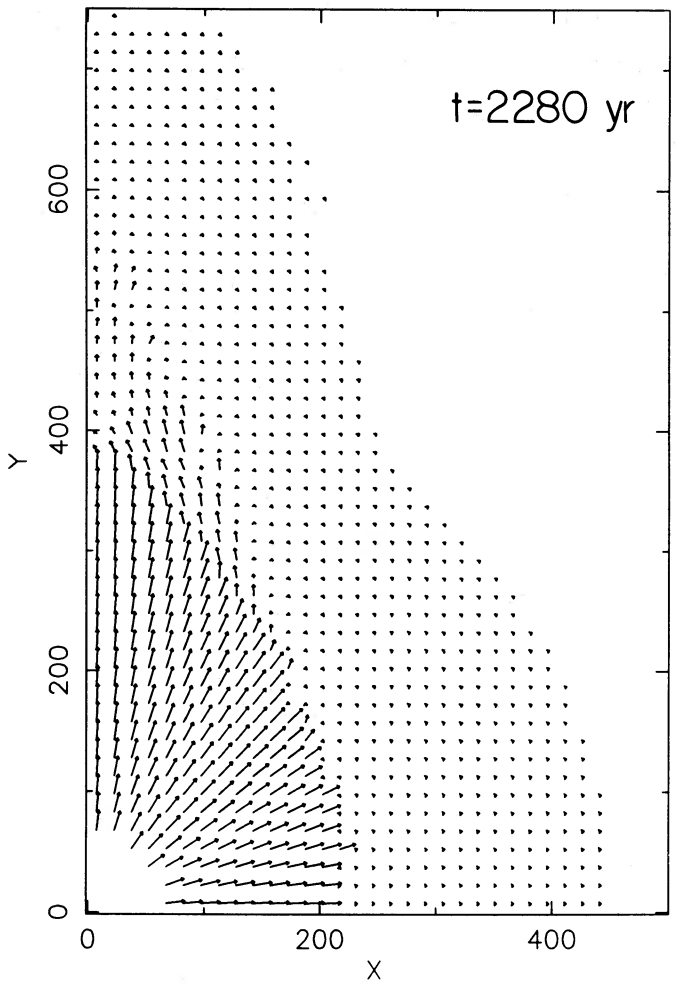

FIG. 5c

FIG. 5.—(*c*) The same as Fig. 5*a*, at $t = 2280$ yr. Each unit length of the arrows corresponds to a velocity of 60 km s^{-1}.

We would like to thank the Pittsburgh Supercomputer Center for providing computing time on a Cray supercomputer. This work has been supported in part by the Kline Prize for Outstanding Research at the Technion, by NASA Astrophysical Theory Center Grant NAGW-764 and by the Fund for the Promotion of Research at the Technion.

REFERENCES

Balick, B. 1987, *A.J.*, **94**, 671.
Balick, B., Preston, H. L., and Icke, V. 1987, *A.J.*, **94**, 1641.
Blakes, J. C., Wheatley, J. M., Panagia, N., Grewing, M., Pettini, M., and Wamsteker, W. 1988, preprint.
Bochkarev, N. G. 1988, *Nature*, **332**, 518.
Bodenheimer, P., and Taam, R. E. 1984, *Ap. J.*, **280**, 771.
Bond, H. E., and Livio, M. 1989, in preparation.
Calvert, N., and Peimbert, M. 1983, *Rev. Mexicana Astr. Ap.*, **5**, 319.
Cassatella, A. 1987, in *SN 1987A*, ed. J. I. Danziger (Garching bei Munchen: ESO), p. 101.
Chevalier, R. A., and Imamura, J. N. 1983, *Ap. J.*, **270**, 554.
Chevalier, R. A., and Soker, N. 1989, *Ap. J.*, in press.
Friend, D. B., and Abbott, D. C. 1986, *Ap. J.*, **311**, 701.
Giuliani, J. L. 1981, *Ap. J.*, **245**, 903.
Harlow, F. H. 1964, in *Methods of Computational Physics*, ed. B. Adler, S. Fernbach, and M. Rotenberg, Vol. **3**, *Fundamental Methods in Hydrodynamics* (New York: Academic), p. 319.
Henler, G. 1982, *Astr. Ap.*, **114**, 309.
Iben, I., Jr. 1984, *Ap. J.*, **277**, 333.
Iben, I., Jr., and Tutukov, A. V. 1988, preprint.
Kahn, F. D. 1983, in *IAU Symposium 103, Planetary Nebulae*, ed. D. R. Flower (Dordrecht: Reidel), p. 305.
Kahn, F. D., and West, K. A. 1985, *M.N.R.A.S.*, **212**, 837.
Kolesnik, I. G., and Pilyugin, L. S. 1986, *Soviet Astr.*, **30**, 169.
Kwok, S. 1982, *Ap. J.*, **258**, 280.
Livio, M. 1982, *Astro. Ap.*, **109**, 37.
Livio, M., Salzman, J., and Shaviv, G. 1979, *M.N.R.A.S.*, **188**, 1.
Livio, M., and Soker, N. 1988, *Ap. J.*, **329**, 764.
Livio, M., Soker, N., deKool, M., and Savonije, G. J. 1986*a*, *M.N.R.A.S.*, **218**, 593.
———. 1986*b*, *M.N.R.A.S.*, **222**, 235.
MacLow, M. M., McCray, R., and Norman, M. L. 1988, preprint.
Perinotto, M. 1983, *IAU Symposium 103, Planetary Nebulae*, ed. D. R. Flower (Dordrecht: Reidel), p. 323.
Poe, C. H., and Friend, D. B. 1986, *Ap. J.*, **311**, 317.
Raymond, J. C. 1988, *Nature*, **332**, 386.
Schonberner, D. 1983, *Ap. J.*, **272**, 708.
Soker, N., Regev, O., Livio, M., and Shara, M. M. 1987, *Ap. J.*, **318**, 760.
Volk, K., and Kwok, S. 1985, *Astr. Ap.*, **153**, 79.
Waters, L. B. F. M. 1986, *Astr. Ap.*, **162**, 121.
Weaver, R., McCray, R., Castor, J., Shapiro, P., and Moore, R. 1977, *Ap. J.*, **218**, 377.
Weiss, A., Hillebrandt, W., and Truran, J. W. 1988, *Astr. Ap.*, **197**, L11.
Zuckerman, B., and Gatley, I. 1987, preprint.

MARIO LIVIO: Department of Physics, Technion, Haifa 32000, Israel

NOAM SOKER: Department of Astronomy, University of Virginia, P.O. Box 3818, University Station, Charlottesville, VA 22903